WEC-Sim Modeling of Laminar Scientific's Patented Seesaw Wave Energy Converter

Preprint

Chelsea Kimball,[1] Salman Husain,[1] Adam Keester,[2] and Narayan Iyer[3]

1 National Renewable Energy Laboratory
2 Sandia National Laboratories
3 Laminar Scientific

Presented at UMERC + METS Marine Energy Research Conference
Duluth, Minnesota
August 7–9, 2024

NREL is a national laboratory of the U.S. Department of Energy
Office of Energy Efficiency & Renewable Energy
Operated by the Alliance for Sustainable Energy, LLC

This report is available at no cost from the National Renewable Energy Laboratory (NREL) at www.nrel.gov/publications.

Contract No. DE-AC36-08GO28308

Conference Paper
NREL/CP-5700-90230
September 2024

WEC-Sim Modeling of Laminar Scientific's Patented Seesaw Wave Energy Converter

Preprint

Chelsea Kimball,[1] Salman Husain,[1] Adam Keester,[2] and Narayan Iyer[3]

1 National Renewable Energy Laboratory
2 Sandia National Laboratories
3 Laminar Scientific

Suggested Citation
Kimball, Chelsea, Salman Husain, Adam Keester, and Narayan Iyer. 2024. *WEC-Sim Modeling of Laminar Scientific's Patented Seesaw Wave Energy Converter: Preprint*. Golden, CO: National Renewable Energy Laboratory. NREL/CP-5700-90230. https://www.nrel.gov/docs/fy24osti/90230.pdf.

NREL is a national laboratory of the U.S. Department of Energy
Office of Energy Efficiency & Renewable Energy
Operated by the Alliance for Sustainable Energy, LLC

This report is available at no cost from the National Renewable Energy Laboratory (NREL) at www.nrel.gov/publications.

Contract No. DE-AC36-08GO28308

Conference Paper
NREL/CP-5700-90230
September 2024

National Renewable Energy Laboratory
15013 Denver West Parkway
Golden, CO 80401
303-275-3000 • www.nrel.gov

NOTICE

This work was authored in part by the National Renewable Energy Laboratory, operated by Alliance for Sustainable Energy, LLC, for the U.S. Department of Energy (DOE) under Contract No. DE-AC36-08GO28308. Funding provided by U.S. Department of Energy Office of Energy Efficiency and Renewable Energy Water Power Technologies Office. The views expressed herein do not necessarily represent the views of the DOE or the U.S. Government. The U.S. Government retains and the publisher, by accepting the article for publication, acknowledges that the U.S. Government retains a nonexclusive, paid-up, irrevocable, worldwide license to publish or reproduce the published form of this work, or allow others to do so, for U.S. Government purposes.

Cover Photos by Dennis Schroeder: (clockwise, left to right) NREL 51934, NREL 45897, NREL 42160, NREL 45891, NREL 48097, NREL 46526.

WEC-Sim modeling of Laminar Scientific's patented seesaw wave energy converter

Chelsea Kimball,[a,*] Salman Husain,[a] Adam Keester,[b] and Narayan Iyer[c]

[a] *National Renewable Energy Laboratory, 15013 Denver West Parkway, Golden, CO 80401 USA*
[b] *Sandia National Laboratories, 1515 Eubank SE, Albuquerque, NM 87123 USA*
[c] *Laminar Scientific, Atlanta, GA 30332 USA*

Abstract

Laminar Scientific's patented seesaw wave energy converter was modeled in WEC-Sim to predict performance. The device operates by utilizing ocean surface waves to rotate a truss in pitch about a pivot. The pivot is located at the top of two pylons, which are embedded in the seafloor. The seesaw has a float on either end, and the buoyancy forces from each float cause the system to rise or fall with passing waves. Device performance relies upon seesaw length and ocean wavelength creating an antiphase effect. The seesaw truss has an adjustable length intended to achieve this effect. The operation method enforces a narrow band of wavelengths which induce the largest rotational motion from the device.

The hydrodynamic analysis of the device was performed using Capytaine, and the results confirmed that the device operates best in a narrow frequency band. Four float-to-float spacing cases and three pylon radii were examined. The hydrodynamic results indicate a match between the model and the physical expectations for the device, and that varying the pylon radii by 0.1-m increments for three instances creates minimal changes in hydrodynamic properties. Power matrices for three float spacing cases of the device were simulated with Joint North Sea Wave Project spectra waves and optimal power take-off damping in WEC-Sim. The maximum average power production for the 15-m spacing case was 14.1 kW with a 5.0-s peak wave period and 4-m significant wave heights. Plots of capture-width ratios indicated that the device performance was linear and confirmed that the device is optimal in a narrow frequency band. The maximum percentage of the available wave power produced by the 15-m device was approximately 16%. Simulations of the device in regular waves were used to produce plots of average power compared to a ratio of float spacing to wavelength. These plots indicate that the power production is maximized at a ratio of 0.5, and further confirm that the device has a narrow frequency response. The device was simulated at an example field location, where the device produced an annual average power rating of 1.6 kW given an average omnidirectional wave climate of 10.3 $kW \cdot m^{-1}$ and an optimal, linearized power take-off model.

While the maximum predicted device performance is reliant upon a narrow band of wave frequencies, the conducted analysis provides an opportunity to improve device design prior to prototyping and testing. Modifying the design to respond to a broader frequency range would improve device performance.

Keywords: WEC-Sim, numerical modeling, wave energy

1. Introduction

Wave energy is currently an untapped renewable resource in the United States. There is enough available power in ocean waves in the exclusive economic zone to provide 34% of U.S. energy needs [1]. With the lack of industrial wave energy converters (WECs) currently connected to the U.S. energy grid, there is ample opportunity to supply a significant portion of U.S. energy requirements with wave power. Additionally, WECs have not yet converged to an optimal design [2], giving novel WECs the potential to fill this technological gap. Novel technologies require evaluation to understand performance prior to prototyping and testing, which are typically resource-intensive practices. Laminar Scientific's patented seesaw WEC was

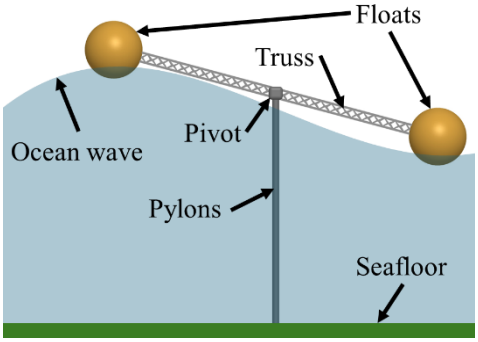

Figure 1. Laminar Scientific's patented seesaw wave energy converter conceptual design (15-m spacing case)

* Corresponding author
Email address: Chelsea.Kimball@nrel.gov

hydrodynamically analyzed and simulated in the ocean environment using both Capytaine and WEC-Sim to produce a numerical model and prediction of device performance.

The Laminar Scientific seesaw WEC comprises two surface-piercing, spherical floats on either end of an adjustable truss assembly (Figure 1). A pivot point at the center of the truss connects the seesaw to two 10-m tall pylons embedded in the seafloor. The 2.6-m diameter spherical floats intermittently rise and fall as ocean waves excite the device. The alternating pitch motion of the truss energizes a power take-off (PTO) system. By controlling the distance between the two surface floats, the Laminar Scientific team hypothesized that energy extracted from varying wave conditions could be increased.

2. Methodology

2.1. Boundary element method (BEM)

To perform the BEM hydrodynamic analysis, the software program Capytaine was utilized [3], while Anaconda [4] was used to install the required Python environment [5]. The pylons were modeled together as a single, rigid body, and the spheres were modeled together as a single, rigid body. The truss was not represented in the BEM solution. Meshes for the bodies were constructed such that the spherical floats had 48 panels along a meridian, and the cylindrical pylons had 20 panels along the circumference and 40 panels along the height. These mesh resolutions were selected to reduce computational runtimes while maintaining hydrodynamic accuracy. Iterative analyses were conducted to produce results for various float-to-float spacings, with main cases of interest being 6 m, 9 m, 12 m, and 15 m. Three pylon radii were examined for each float spacing case: 0.15 m, 0.25 m, and 0.35 m. Frequencies of interest for the analysis included values between approximately 0.4 and 1.6 rad·s^{-1}, corresponding to wave periods between 4 and 16 s. The BEM analysis plots were calculated using WEC-Sim's BEMIO functionality [6].

2.2. WEC-Sim Simulink model

WEC-Sim requires MATLAB and Simulink to operate [7]. To develop the WEC-Sim Simulink model of the seesaw device, the WEC-Sim OSWEC tutorial was used as reference [6]. The model consists of the seabed, fixed pylons, a rotational PTO, and the hydrodynamic body representing the seesaw. Model inputs included a fixed constraint location for the pylons at 0, 0, −10 m, where the coordinates correspond to *x*, *y*, and *z* directions. The PTO location was specified as 0, 0, 0.29 m in the Laminar Scientific design. The linear PTO model includes a damping coefficient applied to rotational motion.

2.3. WEC-Sim Multiple Condition Runs (MCR)

Power matrices of the device were created by employing the WEC-Sim MCR feature. Float spacings of 9, 12, and 15 m were used in this analysis. Each simulation recorded the average power produced by the PTO over a 3,000-s period, with a sampling interval of 0.05 s. The simulation runtime and sampling rate were chosen to ensure accuracy and convergence of average values [8]. The absolute value of power is averaged because the rotational PTO block generates power positively in only one direction. Joint North Sea Wave Project (JONSWAP) wave spectra were applied to each simulation, where significant wave heights and peak periods were modified for each iteration. Significant wave heights varied between 0.5 and 4 m in 0.5-m steps, and peak periods varied between 2 and 9 s in 1-s intervals. The MCR for each spacing created 64 simulations, for a total of 192 simulations. The weight of the rotating body was 4,000 kg, and moments of inertia for each spacing case are included in Table A-1.

For each iteration using the MCR, inputs included optimal PTO damping and hydrostatic stiffness. These were calculated for each simulation using Equation 1 (terms defined in Appendix A):

$$C_{opt} = B(\omega)\sqrt{1 + \left(\frac{K_H - \omega^2(M + A_\infty)}{\omega B(\omega)}\right)^2} \quad (1)$$ [9].

The power matrix results were used to determine the capture-width ratio (CWR) of the device. The CWR reflects the power produced by the device as a percentage of available wave power. Average available wave power is calculated by WEC-Sim during the simulation and is multiplied by the spherical float diameter (2.6 m). The wave

conditions that correspond to breaking waves were identified on the power matrix and CWR plots by a red outline (Figure 4). Breaking waves were considered to occur when the wave steepness ratio exceeded 7^{-1} [10].

The ratio of float-to-float spacing to wavelength was varied and simulated in regular waves to determine what effect the ratio has on average device power. Ratios were chosen between 0.2 and 2 in intervals of 0.1. The wave field was changed from JONSWAP spectra to regular waves, and the remaining simulation parameters were consistent. Because linearity was observed in the system (Figure 4), one wave height (0.5 m) was chosen for this analysis. Additionally, the wave height of 0.5 m would not induce wave breaking for the wave periods examined. Using the chosen wavelengths, wave periods were calculated from the dispersion relationship from linear wave theory (terms defined in Appendix A):

$$\lambda = \frac{gT^2}{2\pi}\tanh\left(\frac{2\pi d}{\lambda}\right) \; or \; T = \sqrt{\frac{2\pi\lambda}{\mathrm{g}\tanh\left(\frac{2\pi d}{\lambda}\right)}} \quad (2)$$ [11].

To predict the annual power performance of the seesaw device with 15-m distance between floats, a coastal location was chosen in the United States with a wave energy period near 5 s, 10-m water depth, and relatively large significant wave height. The Marine Energy Atlas [12] and navigational chart 13237 from the National Oceanic and Atmospheric Administration (NOAA) [13] were used to make the location selection. South of Nantucket in Massachusetts, USA, met the criteria at coordinates 41.22N, −70.20W (see Figure A-1). The energy period, significant wave height, and omnidirectional wave power for the chosen location for monthly averages are included in Table A-2 [12]. The annual average omnidirectional wave power at this location is 10.3 kW·m^{-1} [12].

The method to convert energy period to peak wave period for JONSWAP spectra waves is included in Appendix A. Using peak wave period and the significant wave height as simulation wave field parameters, WEC-Sim MCR produced 12 simulations. The simulation parameters remained the same as previous JONSWAP spectra analyses. Optimal PTO damping and hydrostatic stiffness were calculated for each case. The 12 average power values were averaged to create an indicator of yearly average power expected from the device at the study location.

3. Results

The normalized radiation damping in pitch motion for the seesaw device is shown in Figure 2, left. There are four float-to-float spacings shown, and for each spacing there are three pylon radii. The largest spacing has larger radiation damping values, and these values decrease as the spacing decreases. The three pylon radii for each spacing case have minimal effect on the radiation damping. For the wave frequencies of interest, marked by the gray area, the larger pylon radii have a larger radiation damping. However, this is a minimal effect compared to the float spacing.

The normalized radiation impulse response functions (IRFs) in pitch for the seesaw device are shown in Figure 2, right. There are four float-to-float spacings shown, and a single pylon radius for each. The varying pylon radii between 0.15 and 0.35 m for this case had minimal effect on the IRF results and are therefore not shown. In the normalized radiation IRF, the largest spacing has the largest initial result. All four cases reduce to oscillate about zero within 5 s, indicating stability in the hydrodynamic analysis.

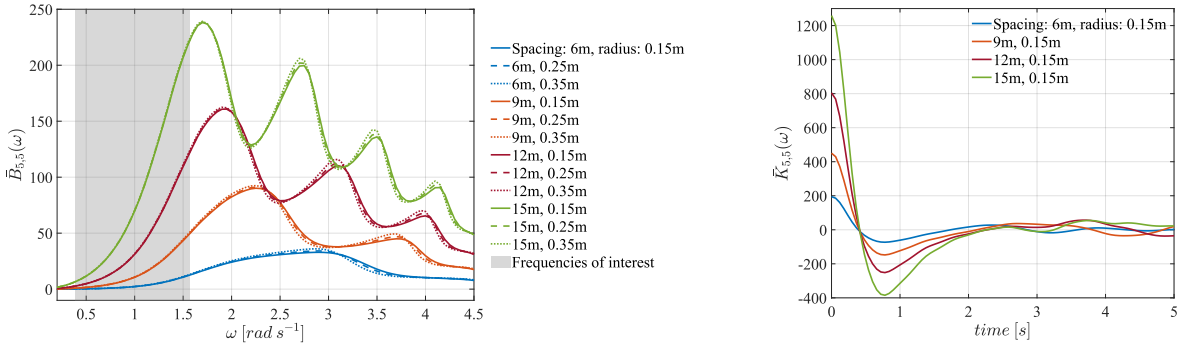

Figure 2. Left: Normalized radiation damping in pitch for the seesaw device. Four float-to-float spacings and three pylon radii were used for 12 total configurations. Wave frequencies of interest are highlighted on the plot in gray. Right: Normalized radiation impulse response functions in pitch for the seesaw device. Four float-to-float spacings and one pylon radius were used.

The excitation force magnitude in pitch was normalized by half the float-to-float spacing for each case, shown in Figure 3. The four spacing cases are shown, and the varying pylon radii cases are excluded due to having minimal effect. Scaling the excitation force in pitch by the lever arm indicates how the vertical wave forces at the floats change, independent of the lever arm increasing torque at the joint. At higher frequencies, the magnitude decreases, which is expected. A peak in excitation force occurs for the 15-m spacing case at approximately 1.3 rad·s^{-1}, or a wave period of 4.8 s. For the smaller spacing cases, this peak in excitation force occurs at marginally higher frequencies, or smaller wave periods.

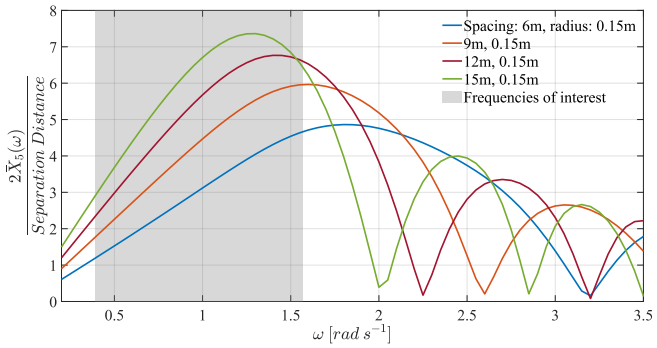

Figure 3. Normalized excitation force magnitude scaled by the seesaw device lever arm, defined as half the float-to-float spacing. Four float-to-float spacings were used. Wave frequencies or periods of interest are shaded in gray.

The added mass and excitation IRFs were examined for the 12 cases and appeared as expected (see Appendix B). The pylon radii examined for each spacing case had minimal effect on overall device hydrodynamics, as shown in the BEM analysis. For this reason, the following sections include only the 0.15-m pylon radius case to reduce the number of total simulations in the analysis. The frequencies of interest were changed to wave periods between 2 and 9 s (from between 4 and 16 s) to capture the largest device response. The 6-m float-to-float spacing case was also not considered for the WEC-Sim analyses by request from Laminar Scientific.

The power matrix for the 15-m float spacing case is shown in Figure 4, left. The 12-m and 9-m spacing cases are included in Appendix C. The highest average power production occurs in wave peak periods of 4–6 s at the largest significant wave heights tested. There is a sharp decrease between the 3- and 4-s peak periods, indicating that the device is most responsive in a narrow wave frequency range. This trend is also observed in the 12-m and 9-m cases; however, as the float spacing decreases, the most responsive peak wave period gradually decreases. The red outlines on Figure 4 indicate where wave breaking will occur. In these regions, the device performance is largely overpredicted.

The CWR, or the percentage of available wave power produced by the seesaw device for the 15-m spacing case, is shown in Figure 4, right. The 12-m and 9-m spacing cases for CWR are included in Appendix C. The largest CWR percentage occurs at the 4-s and 5-s peak periods, similar to trends observed in Figure 4, left. The consistency in CWR values within a given peak period indicates both device linearity and the importance of peak wave period to increase power capture. The optimal PTO damping values for the 15-m spacing case, also utilized in the simulations to generate power matrices and CWR percentages, are included in Table A-3.

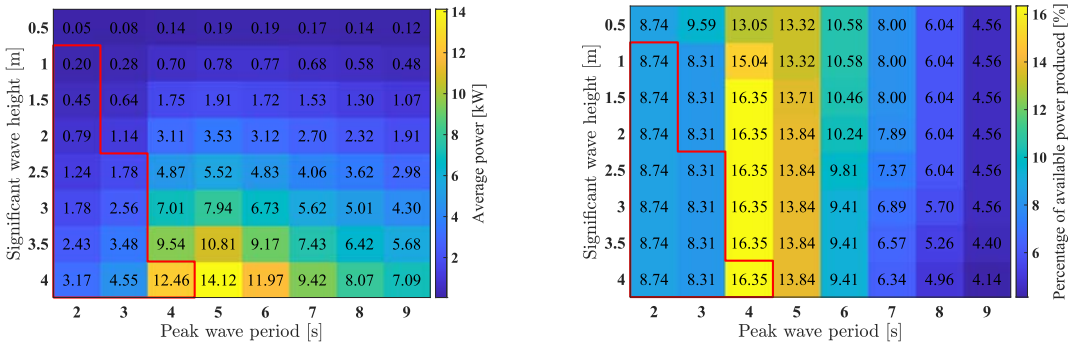

Figure 4. Left: Average power matrix of 15-m-spaced seesaw device simulated in WEC-Sim using JONSWAP spectra waves, with optimized PTO damping for pitch motion. Significant wave heights range from 0.5 to 4 m, and peak periods range from 2 to 9 s. Red outline indicates breaking wave conditions. Right: CWR, or percent of average available wave power produced by 15-m-spaced seesaw device.

The ratio between the float-to-float spacing cases of the seesaw device and the regular waves' wavelengths was iteratively evaluated for average power in Figure 5, left. The range of wave periods to determine the wavelength for each ratio varies from 8.4 to 2.2 s. The average power values peak at the 0.5 and 1.5 ratios. These local maxima indicate the required inherent antiphase behavior, where one float is at a wave crest while the other is at a wave trough, to produce maximum power from the device. Similarly, if the wavelength causes both floats to be collocated vertically, there is no power produced and the device will have minimal regular motion. The largest maximum occurs at a ratio of 0.5, or for the 15-m spacing case, a regular wave period of 4.5 s. While Figure 5, left, was produced using regular waves, this wave period associated with maximum antiphase behavior is similar to trends observed in Figure 4. As the spacing between floats decreases, the average power also decreases for all wave periods less than 6 s.

Examining the maximum power production case for the regular waves (wave period: 4.5 s, wave height: 0.5 m), the power decreases by approximately 66% on average for the three spacing cases when switching from regular to JONSWAP wave spectra, with all other simulation parameters held constant.

The results of the seesaw device simulated near Nantucket, Massachusetts, are shown in Figure 5, right. The yearly average power for the seesaw device is 1.6 kW. The average power fluctuates throughout the year and is highest during the winter months. When compared to the wave conditions, there is a positive scaling effect between power produced and significant wave height. The CWR indicates that the device is utilizing approximately 11% of the available wave power throughout the year. This value inversely scales with peak wave period.

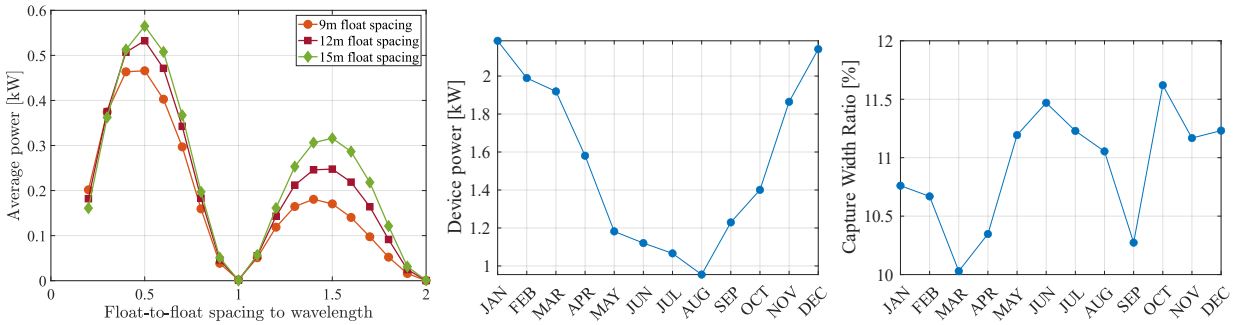

Figure 5. Left: Average power of three float spacing cases in regular wave conditions. Wave height was 0.5 m, and periods were chosen to reflect a float-to-float spacing-to-wavelength ratio between 0.2 and 2 (8.4 to 2.2 s). Right: Monthly average values for the seesaw device performance at the case study location south of Nantucket, MA.

4. Conclusion

The BEM results indicate the hydrodynamic analysis matches the physical expectations for the device. Additionally, results showed that varying the pylon radius between 0.15 and 0.35 m had minimal effect on the hydrodynamics when compared with the varying float spacing. The power matrix results for the three spacing cases indicate that the best conditions for producing power occur at wave peak periods between 3 and 6 s depending upon the float spacing case, for JONSWAP wave spectra and with optimized PTO damping. The best conditions had the largest significant wave height while using a resonant peak period. The maximum average power produced by the 15-m spacing case was 14.1 kW and occurred during the 5-s peak period and 4-m significant wave height. The CWR plots for the three spacing cases indicate that the device performs linearly, and that performance relies upon a narrow range of peak wave periods.

The average power comparison with spacing-to-wavelength ratio further supports this deduction of a narrow-banded response for the device. In regular waves, peak production occurs when the two floats are exactly out of phase (i.e., when one float is at a wave crest while the other float is at a wave trough). Power production is maximized when the float spacing-to-wavelength ratio is 0.5. The increased power production in regular waves compared to the JONSWAP wave spectra cases demonstrates the dependence of the device upon regularity of antiphase behavior for maximizing power production.

A sample field location was selected to simulate the 15-m spacing case device. Because the device has both a low and narrow resonant frequency, geographically positioning the device to maximize power production is difficult.

Yearly average wave conditions south of Nantucket, Massachusetts, include wave energy periods of 5.0 s and significant wave heights of 1.4 m, and the simulated device produced a yearly average power of 1.6 kW.

Finding deployment locations that match the device's resonant frequency, and have large wave heights, could aid in increasing device power performance. Device design alterations could also increase power performance, such as allowing for two rotating lever arms about the pivot point instead of a single, rigid lever arm (used in the Wave Star design).

Acknowledgements

Sandia National Laboratories is a multimission laboratory managed and operated by National Technology & Engineering Solutions of Sandia, LLC, a wholly owned subsidiary of Honeywell International Inc., for the U.S. Department of Energy's National Nuclear Security Administration under contract DE-NA0003525.

This work was authored in part by the National Renewable Energy Laboratory, operated by Alliance for Sustainable Energy, LLC, for the U.S. Department of Energy (DOE) under Contract No. DE-AC36-08GO28308. Funding provided by the U.S. Department of Energy Office of Energy Efficiency and Renewable Energy Water Power Technologies Office. The views expressed in the article do not necessarily represent the views of the DOE or the U.S. Government. The U.S. Government retains and the publisher, by accepting the article for publication, acknowledges that the U.S. Government retains a nonexclusive, paid-up, irrevocable, worldwide license to publish or reproduce the published form of this work, or allow others to do so, for U.S. Government purposes.

Appendix A. Supplementary information for methodology.

Table A-1. Seesaw moments of inertia for each spacing case

	Float-to-float spacing		
Moments of inertia	15 m	12 m	9 m
I_{xx} [kg·m^2]	1.066×10^5	6.115×10^4	3.113×10^4
I_{yy} [kg·m^2]	1.380×10^3	1.380×10^3	1.380×10^3
I_{zz} [kg·m^2]	1.066×10^5	6.116×10^4	3.113×10^4

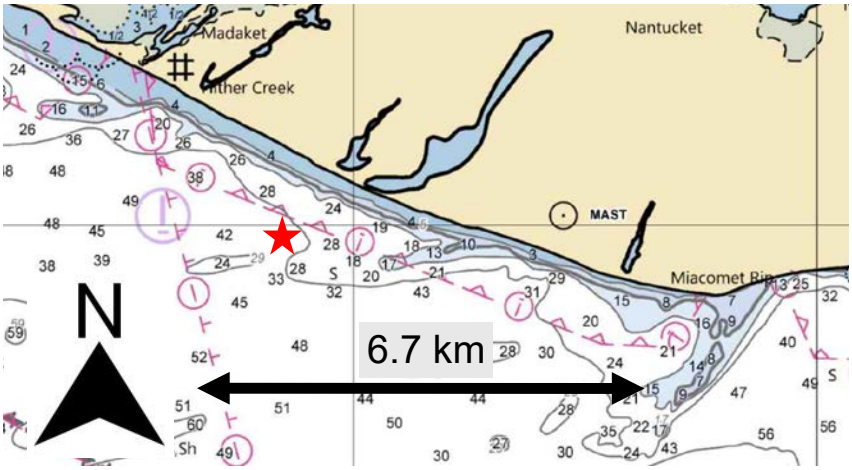

Figure A-1. Section of NOAA chart 13237 showing water depths (in feet) on the southern coast of Nantucket, MA. Red star indicates selected location for the seesaw device in the theoretical case study. Distances are approximate [13].

Table A-2. Monthly average of wave field parameters south of Nantucket, MA [12]

Month	Jan	Feb	Mar	Apr	May	June	July	Aug	Sep	Oct	Nov	Dec
Energy period, T_e [s]	5.1	5.1	5.3	5.2	4.9	4.9	4.9	5.0	5.2	4.8	4.9	5.0
Significant wave height, H_s [m]	1.7	1.6	1.6	1.5	1.2	1.2	1.2	1.1	1.3	1.3	1.6	1.7
Omnidirectional wave power [kW·m^{-1}]	15.2	13.8	14.4	10.6	6.7	5.9	5.7	5.9	9.2	9.2	12.9	14.5

A.1. Conversion of wave energy period to peak wave period for JONSWAP spectra waves

$$T_p = \frac{T_e}{f_{factor}} \quad \text{(A-1) [14],}$$

Where:

T_p = wave peak period [s]
T_e = energy period [s]
f_{factor} = frequency factor $= (0.8255 + 0.03852\gamma - 0.005537\gamma^2 + 0.0003154\gamma^3)$ [14]
γ = peakedness for the single-peak JONSWAP wave model.

When:

$$\frac{T_e}{\sqrt{H_s}} \leq 3.6, \gamma = 5,$$
$$\frac{T_e}{\sqrt{H_s}} > 5, \gamma = 1,$$
$$3.6 < \frac{T_e}{\sqrt{H_s}} \leq 5, \gamma = e^{\left(5.55 - 1.15\left(\frac{T_e}{\sqrt{H_s}}\right)\right)} \quad \text{(A-2) [15],}$$

Where:

H_s = significant wave height = variable [m].

A.2. Optimal damping calculation

$$C_{opt} = B(\omega)\sqrt{1 + \left(\frac{K_H - \omega^2(M + A_\infty)}{\omega B(\omega)}\right)^2} \quad \text{(A-3) [9],}$$

Where:

C_{opt}	= optimal damping coefficient	[N/(m/s)]
$B(\omega)$	= seesaw radiation damping at a given radian frequency	[N/(m/s)]
K_H	= seesaw PTO stiffness (hydrostatic)	[N·rad/m]
ω	= wave radian frequency	[rad/s]
M	= seesaw pitch moment of inertia	[kg]
A_∞	= seesaw pitch added mass as radian frequency approaches infinity	[kg]

Table A-3. Optimal PTO damping values for 15-m spacing case

Peak Period [s]	2	3	4	5	6	7	8	9
Optimal PTO damping [(× 10^6) N/(m/s)]	1.64	2.88	3.99	5.25	6.34	7.86	8.51	10.16

A.3. Dispersion relation from linear wave theory for calculating wavelength or wave period

$$\lambda = \frac{gT^2}{2\pi}\tanh\left(\frac{2\pi d}{\lambda}\right) \text{ or } T = \sqrt{\frac{2\pi\lambda}{g\tanh\left(\frac{2\pi d}{\lambda}\right)}} \quad \text{(A-4) [11],}$$

Where:

λ	= wavelength	= variable	[m]
g	= gravitational acceleration	= 9.81	[m s^{-2}]
T	= wave period	= variable	[s]
d	= water depth at device	= 10	[m]

Appendix B. Additional BEM results

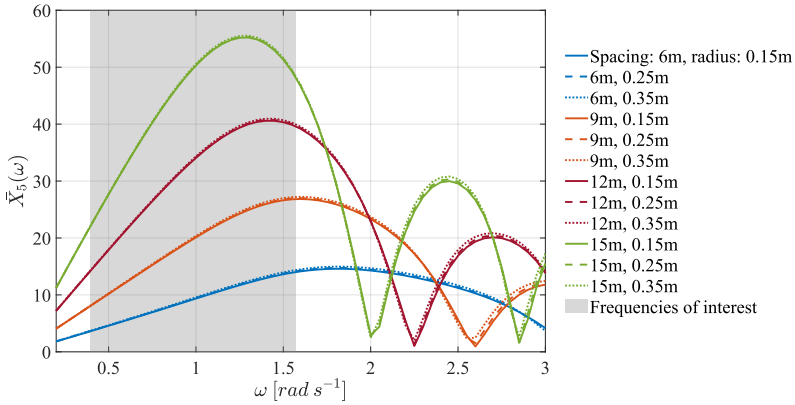

Figure B-1. Normalized excitation force magnitude in pitch for the seesaw device. Four float-to-float spacings and three pylon radii were used for a total of 12 configurations. Wave frequencies or periods of interest are shaded in gray.

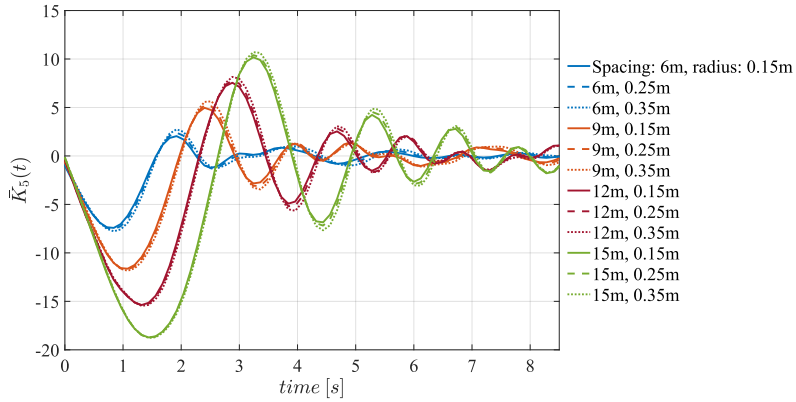

Figure B-2. Normalized excitation impulse response function in pitch for the seesaw device. Four float-to-float spacings and three pylon radii were used for a total of 12 configurations. All configurations reduce to oscillate about zero within 10 s, which is the expected response for this system.

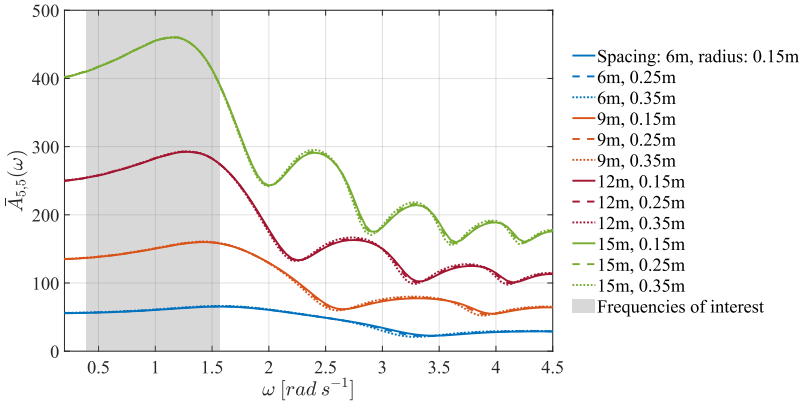

Figure B-3. Normalized added mass in pitch for the seesaw device. Four float-to-float spacings and three pylon radii were used for a total of 12 configurations. Wave frequencies or periods of interest are shaded in gray. The largest added mass occurred in the 15-m spacing case, and peaked at a frequency of approximately 1.2 rad·s^{-1} or a wave period of 5.2 s. For each smaller float spacing case examined, the peak added mass occurred at slightly higher frequencies or smaller wave periods.

Appendix C. Additional power matrices and CWR figures for 12-m and 9-m spacing cases

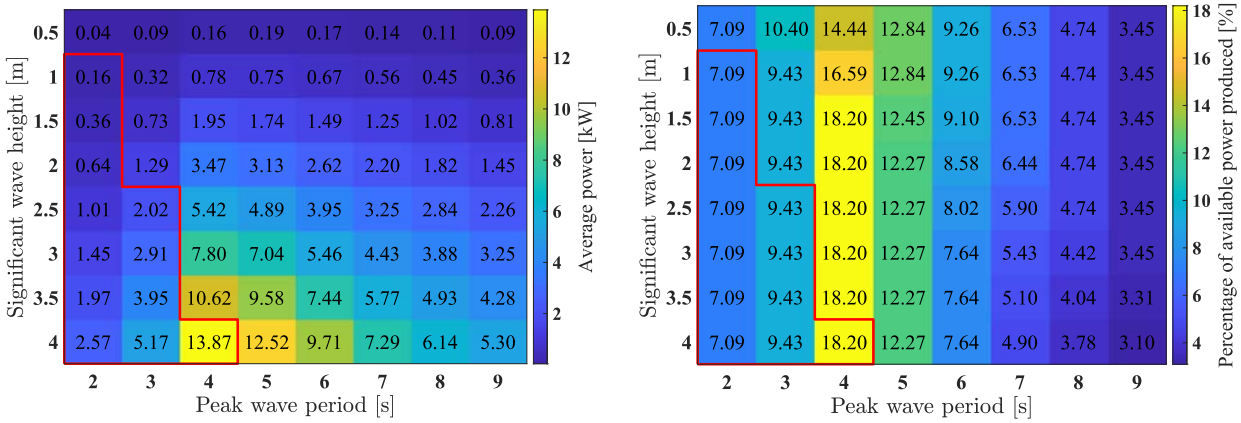

Figure C-1. Left: Average power matrix of 12-m-spaced seesaw device simulated in WEC-Sim using JONSWAP spectra waves, with optimized PTO damping for pitch motion. Significant wave heights range from 0.5 to 4 m, and peak periods range from 2 to 9 s. Red outlines indicate breaking wave conditions. Right: CWR, or percent of average available wave power produced by 12-m-spaced seesaw device.

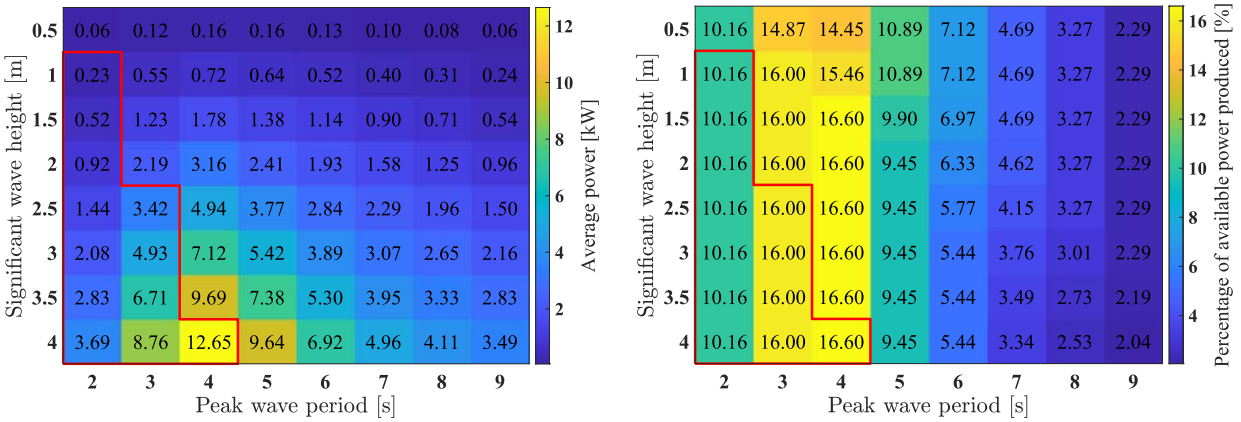

Figure C-2. Left: Average power matrix of 9-m-spaced seesaw device simulated in WEC-Sim using JONSWAP spectra waves, with optimized PTO damping for pitch motion. Significant wave heights range from 0.5 to 4 m, and peak periods range from 2 to 9 s. Red outlines indicate breaking wave conditions. Right: CWR, or percent of average available wave power produced by 9-m-spaced seesaw device.

References

[1] L. Kilcher, M. Fogarty and M. Lawson, "Marine Energy in the United States: An Overview of Opportunities," NREL/TP-5700-78773. National Renewable Energy Laboratory, Golden, CO, 2021. https://www.nrel.gov/docs/fy21osti/78773.pdf.

[2] A. Falcao, "Wave energy utilization: A reviewof the technologies.," *Renewable and Sustainable Energy Reviews,* pp. 899-918, 2010. https://doi.org/10.1016/j.rser.2009.11.003.

[3] M. Ancellin and F. Dias, "Capytaine: a Python-based linear potential flow solver," *Journal of Open Source Software,* pp. 4(36), 1341, 2019. https://joss.theoj.org/papers/10.21105/joss.01341.

[4] "Anaconda Software Distribution," v 23.7.4, 2023. https://anaconda.com.

[5] Python Software Foundation, "Python Language Reference, version 3.11," Available at http://www.python.org.

[6] K. Ruehl, A. Keester, N. Tom, D. Forbush, J. Grasberger, S. Husain, D. Ogden and J. Leon, "WEC-Sim v6.0," 2023. https://doi.org/10.5281/zenodo.10023797.

[7] The MathWorks, Inc, "MATLAB version: 23.2.0 (R2023b)," https://www.mathworks.com.

[8] International Electrotechnical Commission, *TS 62600-101:2015; Marine energy - Wave, tidal and other water current converters - Part 101: Wave energy resource assessment and characterization,* Geneva, Switzerland: IEC, 2015. https://webstore.iec.ch/publication/22593.

[9] N. M. Tom, M. J. Lawson, Y. H. Yu and A. D. Wright, "Development of a nearshore oscillating surge wave energy converter with variable geometry," *Renewable Energy,* vol. 96 Part A, pp. 410-424, 2016. https://doi.org/10.1016/j.renene.2016.04.016.

[10] L. W. Schwartz and J. D. Fenton, "Strongly nonlinear waves," *Annual Review of Fluid Mechanics,* vol. 14, pp. 39-60, 1982. https://doi.org/10.1146/annurev.fl.14.010182.000351.

[11] R. G. Dean and R. A. Dalrymple, Water Wave Mechanics for Engineers and Scientists. Advanced Series on Ocean Engineering, 2, World Scientific Publishing Co, 1991.

[12] National Renewable Energy Laboratory; Sandia National Laboratories; Pacific Northwest National Laboratory, "Marine Energy Atlas," 2020b. [Online]. Available: https://maps.nrel.gov/marine-energy-atlas/.

[13] National Oceanic and Atmospheric Administration, "13237OG Nantucket Sound Nautical Chart".

[14] "The Specialist Committee on Waves Final Report and Recommendations to the 23rd ITTC," in *23rd International Towing Tank Conference*, Venice, Italy, 2002.

[15] International Electrotechnical Commission, *TS 62600-2:2019; Marine energy - Wave, tidal and other water current converters - Part 2: Marine energy systems - Design requirements,* Geneva, Switzerland: IEC, 2019. https://webstore.iec.ch/publication/62399.